Case Rep Ophthalmol 2012;3:434–437
DOI: 10.1159/000346046
Published online: December 22, 2012

ISSN 1663–2699
www.karger.com/cop

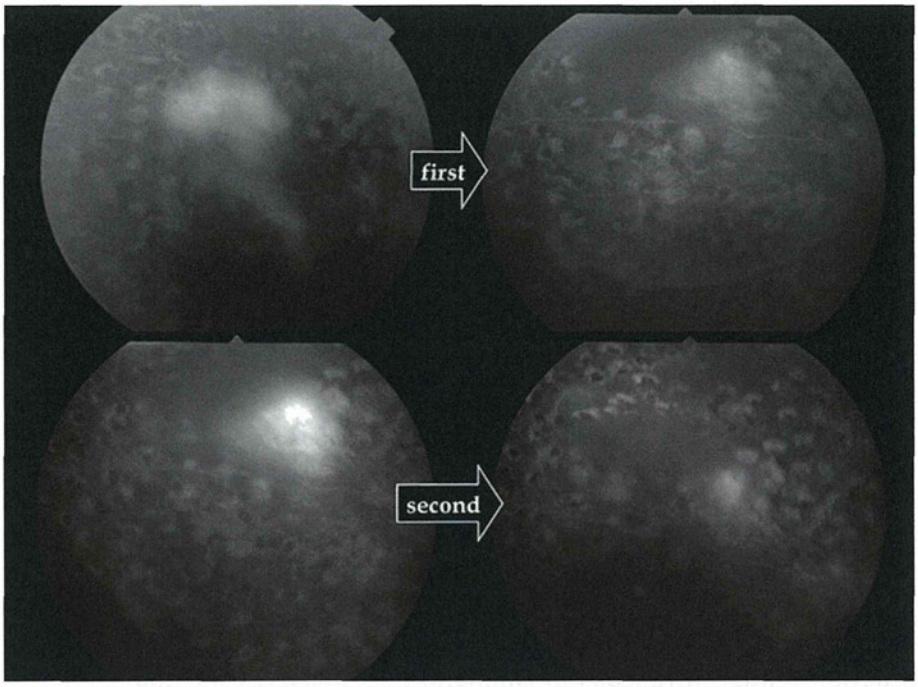

Fig. 2. Change of fluorescein angiography. After IVB, fluorescence leakage decreased markedly from retinal vessels (upper figures: first IVB, lower figures: second IVB).

References

1 Yokoi M, Kase M: Retinal vasculitis due to secondary syphilis. Jpn J Ophthalmol 2004;48:65–67.

2 Gunther JB, Altaweel MM: Bevacizumab (Avastin) for the treatment of ocular disease. Surv Ophthalmol 2009;54:372–400.

3 Aiello LP, Avery RL, Arrigg PG, Keyt BA, Jampel HD, Shah ST, Pasquale LR, Thieme H, Iwamoto MA, Park JE, et al: Vascular endothelial growth factor in ocular fluid of patients with diabetic retinopathy and other retinal disorders. N Engl J Med 1994;331:1480–1487.

4 Mansour AM, Mackensen F, Arevalo JF, Ziemssen F, Mahendradas P, Mehio-Sibai A, Hrisomalos N, Lai TY, Dodwell D, Chan WM, Ness T, Banker AS, Pai SA, Berrocal MH, Tohme R, Heiligenhaus A, Bashshur ZF, Khairallah M, Salem KM, Hrisomalos FN, Wood MH, Heriot W, Adan A, Kumar A, Lim L, Hall A, Becker M: Intravitreal bevacizumab in inflammatory ocular neovascularization. Am J Ophthalmol 2008;146:410–416.

5 Cheung CM, Chee SP: Jarisch-Herxheimer reaction: paradoxical worsening of tuberculosis chorioretinitis following initiation of antituberculous therapy. Eye (Lond) 2009;23:1472–1473.

Case Reports in Ophthalmology

Case Rep Ophthalmol 2012;3:180–184
DOI: 10.1159/000339128

Published online: May 30, 2012

ISSN 1663–2699
www.karger.com/cop

Chickenpox Chorioretinitis with Retinal Exudates and Periphlebitis

Hirokuni Kitamei[a] Kenichi Namba[a] Nobuyoshi Kitaichi[b, c]
Akiko Wakayama[a] Shigeaki Ohno[b] Susumu Ishida[a]

Departments of [a]Ophthalmology and [b]Ocular Inflammation and Immunology, Hokkaido University Graduate School of Medicine, and [c]Department of Ophthalmology, Health Sciences University of Hokkaido, Sapporo, Japan

Key Words
Chickenpox · Chorioretinitis · Intraocular inflammation · Primary VZV infection · Uveitis · Varicella zoster virus · Acute retinal necrosis

Abstract
Background: Chickenpox is rarely associated with posterior segment inflammation. We report on a case of unilateral chickenpox chorioretinitis with retinal exudates and periphlebitis.
Case Presentation: A 21-year-old healthy man, who suffered from chickenpox 2 weeks prior to symptom development, exhibited mild anterior chamber cells, vitreous opacity, sheathing of retinal veins, and yellow-white exudates in his right eye. Varicella zoster virus DNA was detected by polymerase chain reaction in the aqueous humor. He was treated with intravenous acyclovir followed by oral prednisolone and valaciclovir. Aqueous cells quickly disappeared and retinal exudates diminished within 1 month, leaving faint retinal scarring. Retinal arteritis had never been observed in this patient.
Conclusions: Although the ocular findings in this case were similar to acute retinal necrosis (ARN), the clinical features differed from ARN in the following points: (1) mild anterior chamber inflammation, (2) absence of retinal arteritis, and (3) prompt resolution of inflammatory findings. The distinctive clinical features indicated that chorioretinitis associated with chickenpox may not have the same pathological conditions as ARN.

Introduction

Varicella zoster virus (VZV) causes chickenpox at primary infection among children and young adults. After a long incubation period in sensory nerve ganglia, VZV is reactivated and causes herpes zoster and a wide range of neurological diseases [1].

Kenichi Namba
Department of Ophthalmology, Hokkaido University Graduate School of Medicine
N-15, W-7, Kita-ku, Sapporo 060-8638 (Japan)
Tel. +81 11 706 5944, E-Mail knamba@med.hokudai.ac.jp

Case Rep Ophthalmol 2012;3:180–184
DOI: 10.1159/000339128
Published online: May 30, 2012

ISSN 1663–2699
www.karger.com/cop

Ocular inflammations caused by reactivation of VZV include keratitis, iridocyclitis, and acute retinal necrosis (ARN) [2].

Chickenpox, caused by primary VZV infection, is infrequently associated with ocular inflammation, including conjunctivitis, keratitis, and iridocyclitis, and rarely with posterior segment inflammation. Here, we report on a rare case of chorioretinitis complicated with chickenpox and discuss the dissimilarity to ARN by referring to the previous literature.

Case Report

This study was performed with informed consent and followed the guidelines of the Ethics Committee of the Hokkaido University Graduate School of Medicine. A 21-year-old healthy man visited an ophthalmology clinic complaining of floaters and ocular hyperemia in his right eye. Since he was suspected to develop ARN, he was referred to our hospital on the same day.

The patient suffered from chickenpox 2 weeks prior to his ocular symptoms. Fever had already diminished and skin eruptions changed to crusts without medication.

At the first visit, his visual acuity was 20/20 and the intraocular pressure was 18 mm Hg in both eyes. In the right eye, slit-lamp examination detected ciliary injection, 3+ cells in the anterior chamber, mutton-fat keratic precipitates, and Koeppe's iris nodules. Fundus examination revealed slight vitreous opacity, sheathing of retinal veins, and yellow-white exudates. The exudates of 1–3 disc diameters were well demarcated and scattered in all quadrants of the peripheral retina (**fig. 1**, **fig. 2**a, b). Fluorescein angiography showed no leakage from the optic disc and retinal vessels and no avascular area (fig. 2c). His left eye showed no symptoms of inflammation.

Both serum anti-VZV immunoglobulin M and immunoglobulin G antibodies were elevated to 3.7 M.I. and 21.0 G.I., respectively (cut-off level 0–0.9). VZV DNA was detected by polymerase chain reaction from the aqueous humor.

The patient was immediately treated with continuous drip infusion of acyclovir (30 mg/kg/day) for 1 week and oral valaciclovir (20 mg/kg/day) for the following 2 months as well as oral prednisolone (0.6 mg/kg/day), starting 8 days after acyclovir treatment began.

Aqueous inflammatory cells disappeared within a few days. Retinal exudates also shrank immediately and diminished within 1 month, leaving faintly pigmented retinal scarring. Sheathing of retinal veins also disappeared without abnormal changes. The patient has preserved 20/20 or better visual acuity for the following 2 years and has remained free from intraocular inflammation.

Discussion

One of the issues in this case is whether we can call the observed disorder 'ARN' or not. ARN is diagnosed according to the criteria of the Executive Committee of the American Uveitis Society and is characterized by peripheral necrotizing retinitis, retinal arteritis, and a prominent inflammatory reaction in the vitreous and anterior chamber [3]. In the present case, the following two findings were incompatible with these criteria: (1) sheathing of vessels was observed in the retinal veins but not in the arteries, and (2) intraocular inflammation in the anterior segment was mild.

The complication of chorioretinitis with chickenpox has been reported using different diagnostic terms such as 'ARN with chickenpox', 'chickenpox chorioretinitis' or 'varicella chorioretinitis' [4, 5]. Recently, Tajunisah and Reddy [6] reported such a case and reviewed the literature of 16 cases of chorioretinitis following chickenpox,

Case Rep Ophthalmol 2012;3:180–184
DOI: 10.1159/000339128
Published online: May 30, 2012

ISSN 1663–2699
www.karger.com/cop

although they used the term 'ARN complicating chicken pox'. In the majority of these cases, the inflammation was mild and less fulminant with good visual prognosis, and retinal detachment with multiple retinal breaks in the area of exudates never occurred.

Systemic pathological response is immunologically different between primary and reactivated infection of VZV, suggesting that inflamed eyes may show different clinical features. Compared with ARN (a local infection with reactivated VZV), chickenpox (a primary infection with VZV) has higher anti-varicella immune response which may contribute to prompt improvement of ocular inflammation with good visual prognosis. Furthermore, the fact that retinal lesions with exudates hardly cause retinal breaks in chickenpox indicates that pathological changes may not be 'necrotic' in the lesions. Therefore, it may not be accurate to diagnose chorioretinitis complicated with chickenpox as 'ARN'. In order to establish the adequate nomenclature, further accumulation of similar cases is needed.

The present patient complained of only mild symptoms such as slight floaters and hyperemia. Though this case was an adult man, chickenpox commonly affects children. Young children may not complain of these mild symptoms, even if they suffer from chickenpox chorioretinitis. Therefore, both pediatricians and ophthalmologists should pay attention to the ocular condition in children with chickenpox.

Disclosure Statement

None of the authors have a conflict of interest to disclose.

Case Rep Ophthalmol 2012;3:180–184
DOI: 10.1159/000339128
Published online: May 30, 2012

ISSN 1663–2699
www.karger.com/cop

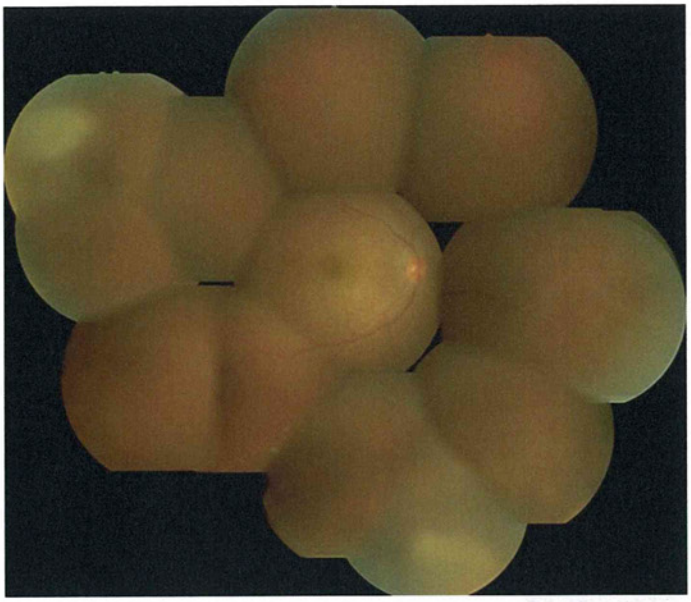

Fig. 1. Fundus photograph of the right eye before treatment. At the first examination, vitreous opacity, sheathing of retinal veins, and yellow-white exudates were observed. The exudates were well demarcated and presented in the peripheral retina and not connected with each other.

Case Rep Ophthalmol 2012;3:180–184
DOI: 10.1159/000339128
Published online: May 30, 2012

ISSN 1663–2699
www.karger.com/cop

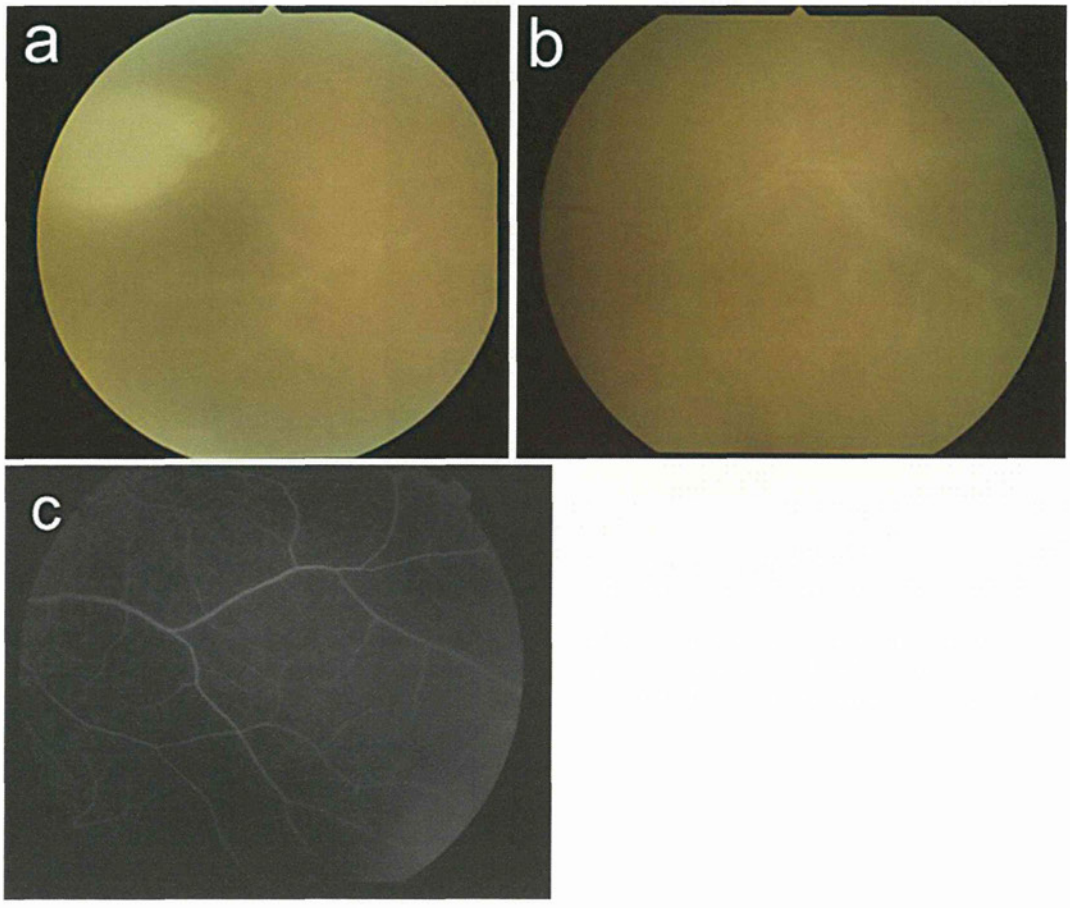

Fig. 2. Higher magnification photographs showed a well-demarcated exudate in the superotemporal retina (**a**) and sheathing of retinal veins in the nasal retina (**b**). Of note is that sheathing was observed in the retinal veins but not in the arteries. Fluorescein angiography showed no fluorescein leakage from the veins (**c**).

References

1 Mueller NH, Gilden DH, Cohrs RJ, Mahalingam R, Nagel MA: Varicella zoster virus infection: clinical features, molecular pathogenesis of disease, and latency. Neurol Clin 2008;26:675–697.

2 Soushi S, Ozawa H, Matsuhashi M, Shimazaki J, Saga U, Kurata T: Demonstration of varicella-zoster virus antigens in the vitreous aspirates of patients with acute retinal necrosis syndrome. Ophthalmology 1988;95:1394–1398.

3 Holland GN: Standard diagnostic criteria for the acute retinal necrosis syndrome. Executive Committee of the American Uveitis Society. Am J Ophthalmol 1994;117:663–667.

4 Kelly SP, Rosenthal AR: Chickenpox chorioretinitis. Br J Ophthalmol 1990;74:698–699.

5 Aslan O, Soykan E, Ozkan SS: Varicella chorioretinitis. Acta Ophthalmol Scand 2007;85:907–908.

6 Tajunisah I, Reddy SC: Acute retinal necrosis complicating chicken pox in a healthy adult: a case report and review of literature. Ann Ophthalmol 2007;39:57–62.

Retina

Quantitative Analyses of High-Resolution 3D MR Images of Highly Myopic Eyes to Determine Their Shapes

Muka Moriyama,[1] Kyoko Ohno-Matsui,[1] Toshio Modegi,[2] Junichi Kondo,[2] Yoichi Takahashi,[2] Makoto Tomita,[3] Takashi Tokoro,[1] and Ikuo Morita[4]

Purpose. We analyzed the symmetry and pointedness of the posterior segment of highly myopic eyes.

Methods. We studied 234 eyes of 117 patients with bilateral high myopia (refractive error ≤−8.00 diopters [D]) and 40 eyes of 20 patients with emmetropia (refractive error between −1.0 and +1.0 D). Volume renderings of high-resolution magnetic resonance (MR) images were performed to obtain 3D images of the eye. To analyze the symmetry and pointedness of the posterior surface, a software was developed to measure the area and angle of a fan-shaped segment formed by selected points on the MR images.

Results. All of the emmetropic eyes were symmetrical in the horizontal and sagittal planes with no deformity. In highly myopic eyes, the shape was symmetrical in the horizontal plane in 146 eyes (62.4%) and in the sagittal plane in 162 (69.2%). The shape of the posterior pole was pointed (angle of fan-shaped segment <150°) in 45.7% and blunted (angle ≥150°) in 54.3% of highly myopic eyes. The most common shape was symmetrical in the horizontal and sagittal planes, and the posterior surface was blunt. The shape of the two eyes of the same individual was the same in 61 of 117 patients (52.1%). In 56 patients whose two eyes had different shapes, the most frequent pattern was a difference in the pointedness (51.8%).

Conclusions. Quantitative assessments of the shape of eyes were useful in determining the pattern of eye shape deformity specific to pathologic myopia. (*Invest Ophthalmol Vis Sci.* 2012;53:4510–4518) DOI:10.1167/iovs.12-9426

Pathologic myopia is a major cause of blindness worldwide.[1–3] Eyes with pathologic myopia not only have elongated axial lengths, but also have different shapes.[4,5] Although the elongation of the eye can be measured by laser instruments, for example IOL Master (Carl-Zeiss, Tubingen, Germany), the shape of the eye has been difficult to determine. Examinations of optical coherence tomographic (OCT) images have been useful; however, only a limited area of the posterior segment of the eye can be examined.

We recently studied the shapes of highly myopic eyes with high-resolution magnetic resonance (MR) imaging with volume rendering of the acquired images.[6] We analyzed the 3-dimensional (3D) topographic images of these eyes and showed that the ocular shape of the highly myopic eyes could be classified into 4 distinct types: nasally distorted, temporally distorted, cylindrical, and barrel-shaped.[6] However, the classification of the shape in that study was based on the subjective judgments of the investigators. Such subjective analysis had a risk of misjudging the eye shape between investigators. In addition, because the differences in the shape can be small, such subjective analysis would make it difficult to follow changes in the eye shape of the same individual with increasing time.

To overcome these problems, we developed a computer program to analyze the eye shape of highly myopic patients obtained from the 3D MR images.

Methods

The procedures used in our study adhered to the tenets of the Declaration of Helsinki, and were approved by the Ethics Committee of Tokyo Medical and Dental University. A written informed consent was obtained from all participants.

We studied 117 patients with bilateral pathologic myopia, defined as a refractive error (spherical equivalent) ≤−8.0 diopters (D) or an axial length >26.5 mm. As controls, 20 individuals with emmetropia (refractive error between −1.0 and +1.0 D) were evaluated in the same way. All emmetropic participants were current or former staff members of the University and all volunteered. The clinical characteristics of the participants are shown in Table 1. Patients with a history of scleral buckling or ocular trauma that could affect the eye shape were excluded.

All participants had comprehensive ocular examinations, including the best-corrected visual acuity (BCVA), refractive error measurements, axial length measurements using IOL Master (Carl-Zeiss), visual fields with a Goldmann perimeter, detailed ophthalmoscopic examinations, fluorescein fundus angiography (FFA), and OCT. The refractive status was measured with an autorefractometer (ARK-730; Nidek, Nagoya, Japan) without cycloplegia, and the BCVA was measured with a chart of Landolt rings set at a distance of 5 m. The decimal BCVAs were converted to the logarithm of minimal angle of resolution (logMAR) units for statistical analyses. The correlation between the eye shape and three representative fundus lesions specific to pathologic myopia, that is myopic choroidal neovascularization (myopic CNV), myopic chorioretinal atrophy, and myopic traction maculopathy (MTM), was determined.

A Cirrus OCT (Carl Zeiss Meditec, Oberkochen, Germany) was used to detect the presence of MTM, and FFA and OCT were used to detect the presence of a myopic CNV. Some of the eyes had visual field defects that were not associated with the three myopic lesions. In these eyes, we examined carefully the relationship between the shapes of the eyes

From the Departments of [1]Ophthalmology & Visual Science and [4]Cellular Physiological Chemistry, Tokyo Medical and Dental University Graduate School of Medicine and Dental Sciences, Tokyo, Japan; [3]Clinical Research Center, Tokyo Medical and Dental University Hospital of Medicine, Tokyo, Japan; and [2]Dai Nippon Printing Co., Ltd., Tokyo, Japan.

Submitted for publication January 3, 2012; revised April 3, May 16, and May 29, 2012; accepted May 29, 2012.

Disclosure: **M. Moriyama**, None; **K. Ohno-Matsui**, None; **T. Modegi**, Dai Nippon Printing Co., Ltd. (E); **J. Kondo**, Dai Nippon Printing Co., Ltd. (E); **Y. Takahashi**, Dai Nippon Printing Co., Ltd. (E); **M. Tomita**, None; **T. Tokoro**, None; **I. Morita**, None

Corresponding author: Kyoko Ohno-Matsui, Department of Ophthalmology and Visual Science, Tokyo Medical and Dental University, 1-5-45 Yushima, Bunkyo-ku, Tokyo 113, Japan; k.ohno.oph@tmd.ac.jp.

Investigative Ophthalmology & Visual Science, July 2012, Vol. 53, No. 8

TABLE 1. Patient and Study Eye Characteristic at the Initial Examination

	High Myopia	Emmetropia
Sex. No. patients (eyes)		
Men	24 (48)	11 (22)
Women	93 (186)	9 (18)
Age (y), mean ± SD	60.0 ± 12.3	52.7 ± 13.2
Refractive error (D), mean ± SD	−15.5 ± 6.1	0.06 ± 0.63
Axial length (mm), mean ± SD	30.3 ± 2.3	23.3 ± 0.7
Baseline logMAR, mean ± SD	0.33 ± 0.48	0.02 ± 0.03

and the visual field defects. The visual fields were quantified by using a grid system proposed by Kwon et al.[7] The grid consisted of 100 sectors that lay within the V4 isopters. The visual field score ranged from 0 (total loss of vision within the V4 isopter) to 100 (normal visual field). We considered eyes with a loss in >10% of the dots to have significant visual field defects as we have reported previously.[8]

MR Imaging

MR imaging examinations and volume rendering of MR images of the eyes were done as reported previously.[6] All patients were examined with a whole-body MR scanner (Signa HDxt 1.5T, version 15; GE Healthcare, Waukesha, WI). To obtain a high-contrast delineation of the border of the eye, the following scanning sequence was performed: fat-suppressed T2-weighted cube, which is an improved sequence of 3D-fast-spin-echo (3DFSE), with the parameters of 256 × 256 matrix, 22 cm field of view, 1.2-mm slice thickness, repetition time (TR) 2500 ms, echo time (TE) 90 ms, and echo train length (ETL) 90. The scan time for each subject was 4 minutes. T2-weighted MRI, which images the intraocular fluid and not the sclera, was used.

Volume renderings of the images were done on a computer workstation (version AW 4.4; GE Healthcare) to obtain high-resolution 3D data. The borders of the globe were identified semi-automatically by the signal intensity, and the tissues on the outside of the globe were removed. The boundary between the retina and vitreous fluid was determined by adjusting the signal intensity in the volume rendering of the MR images. When the signal intensity gradually was increased manually, only the signal from vitreous fluid remained. De-noising, such as smoothing or curve/surface fitting, was done automatically by the computer workstation after the volume rendering of the images was done.

Establishment of Central Axis Line

First, the center of gravity (Pg) was determined by the coordinates of the contour of the shape. Then, one point on the anterior edge of the eye was defined (Pa). Initially, Pg was fixed, and Pa was shifted along the anterior border. Then one point (Pc) on the Pg-Pa line was defined, and Pc was moved to several locations from Pb to Pa in one-pixel steps. The intersection point of the contour and the line crossing orthogonally to Pg-Pa on Pc was defined as P_{+v} and P_{-v}, respectively. Pa was calculated to be when the difference between the length of Pc-P_{+v} and the length of Pc-P_{-v} at each Pc point became a minimum. After the correction of Pa, Pa was fixed and Pg was shifted by changing the Y-coordinate. Any one point (Pc) on the Pg-Pa axis was defined, and then Pg was recalculated in the same way. After the correction of Pa and Pg, the Pa-Pg line was set to be central axis line (Supplementary Figs. 1–6, http://www.iovs.org/lookup/suppl/doi:10.1167/iovs.12-9426/-/DCSupplemental).

Measurement of Eye from 3D MR Image

The views of the eye from 6 directions (anterior, posterior, superior, inferior, nasal, and temporal) were incorporated into the software of the 3D MR image (Fig. 1). A central axis line was drawn automatically through the eye. The following parameters were measured in pixels automatically by the software:

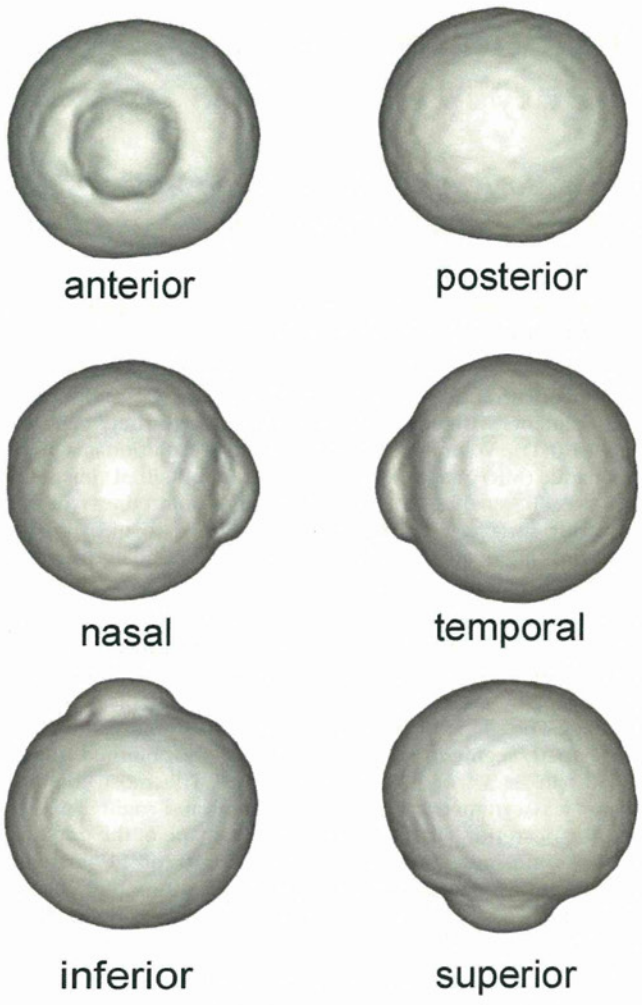

FIGURE 1. The 6 views of the eye that were analyzed by our software. These views are those of a 3D MR image.

1. Sagittal axial length: Length of central axis (Figs. 2, 3; red dotted line).
2. Vertical length of eye: Length of line that crosses orthogonally to the central axis at the midpoint of the sagittal line (Fig. 3B, blue dotted line).
3. Horizontal length of eye: Length of a line that crosses orthogonally to the central axis at its midpoint in the horizontal plane (Fig. 3A, blue dotted line).
4. Posterior basal point (Pb): Point of intersection of the central axis and the posterior edge of the eye.
5. Point of origin (Po): Point on the central axis 87 pixels anterior to Pb, which is approximately 12.5 mm from Pb. This is different from the midpoint of the central axis and was done to avoid the influence of the axial length on the location of Po.
6. P_{+n}: Point on the posterior surface of the eye that is 22.5° nasal (in horizontal plane) or inferior (in sagittal plane) to Po.
7. P_{-n}: Point on the posterior surface of the eye that is 22.5° temporal (in horizontal plane) or superior (in sagittal plane) to Po.
8. P_{+w}: Point on the posterior surface that is 45° nasal (in horizontal planes) or inferior (in sagittal planes) to Po.
9. P_{-w}: Point on the posterior surface that is 45° temporal (in horizontal planes) or superior (in sagittal planes) to Po (Figs. 2, 3).

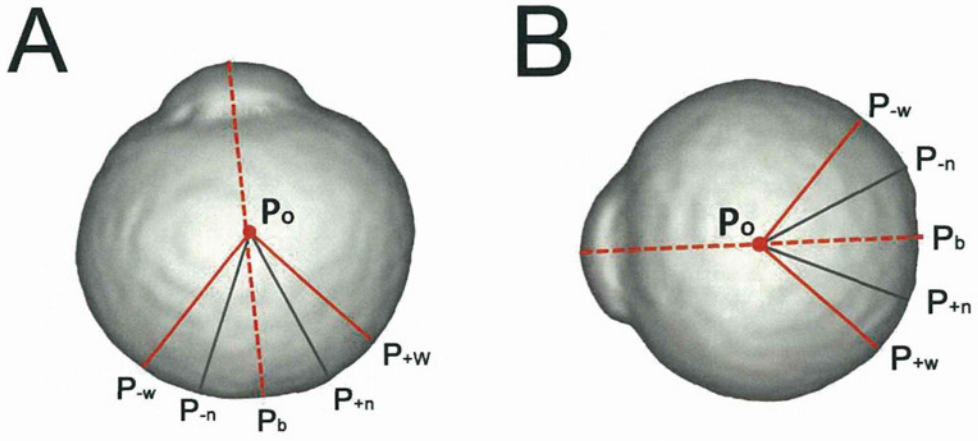

FIGURE 2. The central axis line is drawn automatically (*red dot line*), and the measurement points (P_b, P_o, $P_{\pm n}$, $P_{\pm w}$) also are set automatically. (**A**) Horizontal plane. (**B**) Sagittal plane.

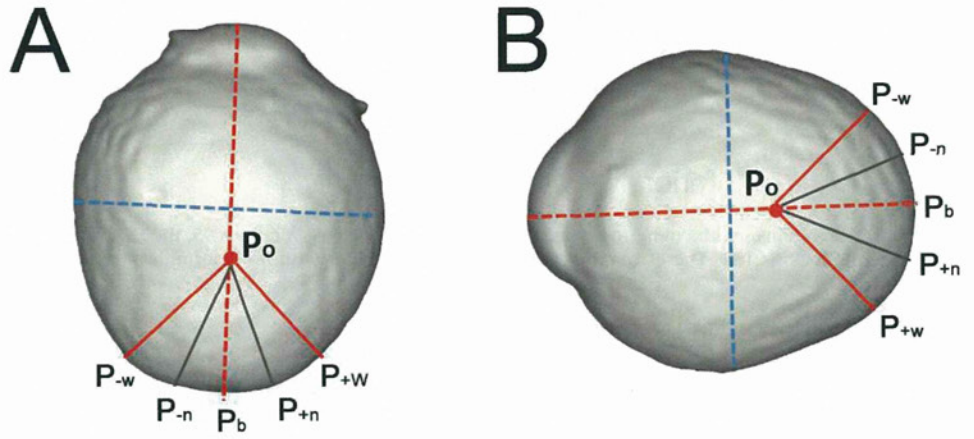

FIGURE 3. The central axis line is drawn automatically (*red dot line*), and the measurement points (P_b, P_o, $P_{\pm n}$, $P_{\pm w}$) also are set automatically. (**A**) The vertical length is shown (*blue dotted line*). (**B**) The horizontal length is shown (*blue dotted line*).

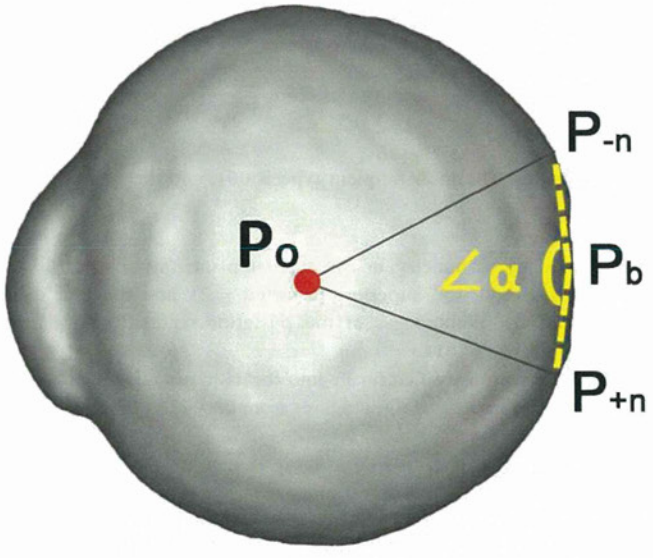

FIGURE 4. The pointedness of the posterior surface is represented by the angle formed by P_{+n}, $-P_b$, and P_{-n} ($\angle\alpha$). The angle was measured for 4 views (nasal, temporal, inferior, superior), and the mean value was adopted as the pointedness of the posterior surface.

The area (in pixels) of the fan-shaped segment formed by Po, Pb, and P_{+n} was defined as S_{+n}, and the segment formed by Po, Pb, and P_{+w} was defined as S_{+w}. S_{-n} and S_{-w} were defined similarly.

Based on these landmarks, the following parameters were calculated and used for the statistical analyses: Ratio of the vertical length to axial length (V/A ratio), ratio of the horizontal length to axial length (H/A ratio), and degree of symmetry of the posterior surface of the eye. The degree of symmetry in the horizontal plane was determined by the ratio of the area of the temporal segment to that of the nasal segment (T/N ratio). $S_{+w} \times 100/S_{-w}$ in the horizontal plane was defined as a wide T/N ratio, and $S_{+n} \times 100/S_{-n}$ as a narrow T/N ratio. For wide and narrow T/N ratios, the ratios that were more apart from 100 were chosen. The eyes whose T/N ratio was >110 were classified as having a temporally-distorted shape, and the eyes whose T/N ratio was <90 were classified as having a nasally-distorted shape. Eyes whose T/N ratio was between 90 and 110 were classified as horizontally symmetrical.

The degree of symmetry in the sagittal plane was determined by the ratio of the area of the superior segment to that of the inferior segment (S/I ratio). $S_{+w} \times 100/S_{-w}$ in the sagittal plane was defined as a wide superior-to-inferior ratio (S/I ratio), and $S_{+n} \times 100/S_{-n}$ as a narrow S/I ratio. For wide and narrow S/I ratios, the ratio that was more apart from 100 was chosen to represent the symmetry in the sagittal plane. The eyes whose S/I ratio was >110 were classified as superior-distorted shape, and the cases whose S/I ratio was <90 were classified as inferior-distorted shape. The cases whose S/I ratio was between 90 and 110 were classified as sagittally symmetrical.

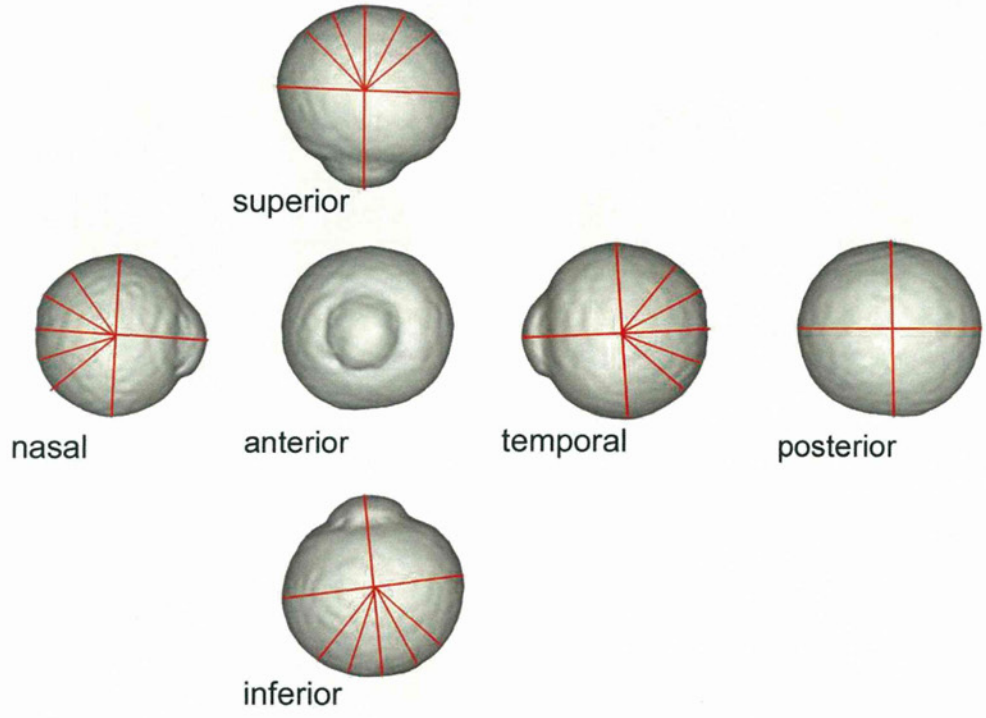

FIGURE 5. The right eye of a 61-year-old man with emmetropia (axial length 24.8 mm). The V/A ratio is 95, the H/A ratio is 100, the T/N ratio is 98, the S/I ratio is 102, and the pointedness is 162. These data indicated that the eye is blunt with no deformities.

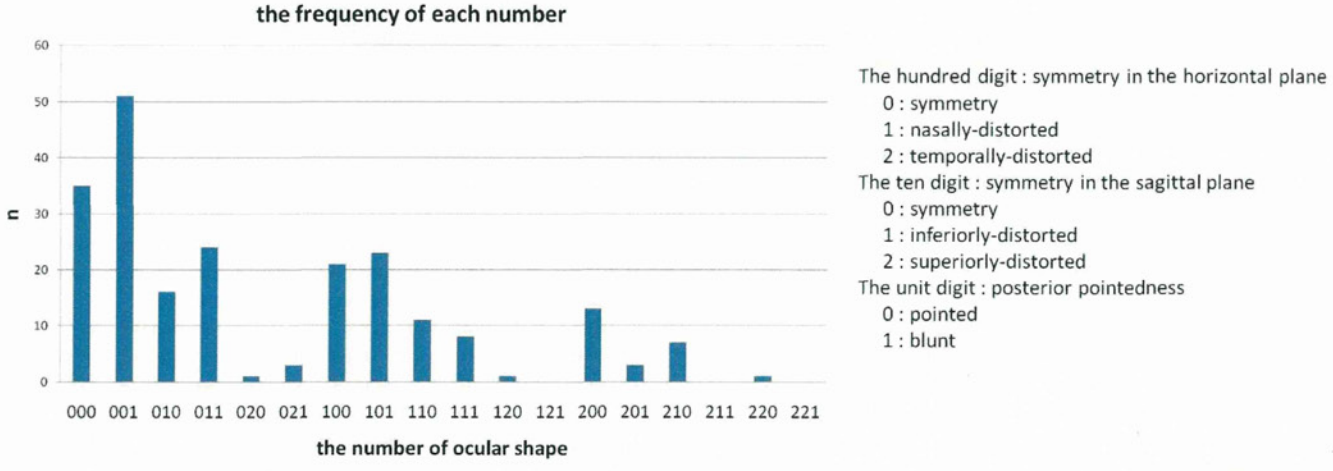

FIGURE 6. Bar graph showing the frequency of the different types of ocular deformities. The most frequent type is 001, and the second most frequent type is 000.

We also calculated the shape of the posterior surface. The angle ($\angle$) formed by P_{+n}-P_b-P_{-n} was defined as the posterior pointedness (Fig. 4). The shape of the posterior segment of the globe was defined as "pointed" when this angle was $<150°$ and "blunt" when this angle was $\geq 150°$.

Deformities of Eye

When an eye was spherical, the V/A and H/A ratios were approximately 100. We defined eyes as not being deformed when the V/A and H/A ratios were both >95.

For the eye whose V/A or H/A ratio was ≤ 95, the deformity of the eye was expressed by a three-digit figure, where the hundreds digit represented the symmetry in the horizontal plane (symmetrical = 0, nasally-distorted = 1, and temporally-distorted = 2), the tens digit represented the symmetry in the sagittal plane (symmetrical = 0, inferiorly-distorted = 1, superiorly-distorted = 2), and the unit digit represented the pointedness of the posterior segment of the eye (pointed = 0, blunt = 1).

The eyes were classified finally into the 18 types according to the different combinations of these figures from 000–221 (Table 2).

Statistical Analyses

The significance of the differences in patients' age, BCVA, axial length, and the parameters of deformities was determined by Student's *t*-tests, Welch's *t*-tests, Mann-Whitney's *U* test and the Kruskal-Wallis test. The frequency of ocular deformity, visual field defects, MTM, CNV, and chorioretinal atrophy was compared using the χ^2 test. The correlation between posterior pointedness and age or axial length was analyzed by

TABLE 2. Summary of 18 Types of Eye Shape

Number	Symmetricity		Shape of Posterior Surface
	In Horizontal Plane	In Sagittal Plane	
000	Symmetrical	Symmetrical	Pointed
001	Symmetrical	Symmetrical	Blunt
010	Symmetrical	Inferiorly-distorted	Pointed
011	Symmetrical	Inferiorly-distorted	Blunt
020	Symmetrical	Superiorly-distorted	Pointed
021	Symmetrical	Superiorly-distorted	Blunt
100	Nasally-distorted	Symmetrical	Pointed
101	Nasally-distorted	Symmetrical	Blunt
110	Nasally-distorted	Inferiorly-distorted	Pointed
111	Nasally-distorted	Inferiorly-distorted	Blunt
120	Nasally-distorted	Superiorly-distorted	Pointed
121	Nasally-distorted	Superiorly-distorted	Blunt
200	Temporally-distorted	Symmetrical	Pointed
201	Temporally-distorted	Symmetrical	Blunt
210	Temporally-distorted	Inferiorly-distorted	Pointed
211	Temporally-distorted	Inferiorly-distorted	Blunt
220	Temporally-distorted	Superiorly-distorted	Pointed
221	Temporally-distorted	Superiorly-distorted	Blunt

Spearman's correlation coefficient rank test. A value of $P < 0.05$ was considered statistically significant.

RESULTS

Eye shape was analyzed by our software successfully in all of the eyes. The time required for the analysis of each 3D MR image was approximately one second. The repeatability of the analysis by the software was confirmed by measuring the parameters of the 3D-MR images taken at different times in 2 individuals, and the results were exactly the same.

Analysis of Emmetropic Eyes

The mean V/A ratio of emmetropic eyes was 99.5 ± 3.5 (range 95.0–104.5) and the mean H/A ratio was 101.2 ± 3.4 (range 95.5–105.0). These data indicated that the axial, vertical, and horizontal lengths were approximately the same, and the shape of emmetropic eyes was spherical. The average T/N ratio was 96.9 ± 4.6 (range 91.0–105.0) and the average S/I ratio was 93.3 ± 3.8 (range 91.0–102.0). The average pointedness of the posterior surface of emmetropic eyes was 157.5 ± 4.4 (range 150–163).

Thus, the shape of emmetropic eyes was symmetrical in the horizontal and sagittal planes, and the posterior shape was calculated to be blunt (Fig. 5). None of the emmetropic eyes had a deformity of the eye shape according to our definition, and the three digit score was 001.

Analysis of Eyes with Pathologic Myopia

In eyes with pathologic myopia, the T/N ratio ranged from 90–110 in 146 of 234 eyes (62.4%), and thus the posterior surface of these eyes was symmetrical in the horizontal plane. A nasally-distorted shape with a T/N ratio <90 was found in 64 eyes (27.4%) and temporally-distorted shape with a T/N ratio >110 was found in 24 eyes (10.3%).

In the sagittal plane, the posterior eye surface was symmetrical, with an S/I ratio of 90–110 in 162 of 234 eyes (69.2%). An inferiorly-distorted shape with an S/I ratio <90 was found in 66 eyes (28.2%), and only 6 eyes (3%) had a superiorly-distorted shape with an S/I ratio >110.

Of 234 eyes 107 (45.7%) had a pointed posterior surface with a P_{+n}-P_b-P_{-n} angle that was <150 degrees, and 127 eyes (54.3%) had a blunt surface with the P_{+n}-P_b-P_{-n} angle that was ≥150 degrees. The P_{+n}-P_b-P_{-n} angle was significantly smaller in the temporally-distorted eyes than in the nasally-distorted eyes or the horizontally-symmetrical eyes (142.5 ± 7.1, 149.2 ± 8.0, and 152.4 ± 8.8, respectively; $P = 1.54 \times 10^{-4}$, Kruskal-Wallis test).

As opposed to the emmetropic eyes, only 6/234 eyes (2.6%) among the 3 highly myopic patients had a V/A and H/A ratio >95. This indicated that they had no deformity in the eye shape. These 3 patients were significantly younger and had shorter axial lengths than the other 114 highly myopic patients (mean age 40.0 ± 6.1 vs. 60.6 ± 12.0 years, $P = 0.01$; and mean axial length 27.9 ± 1.0 vs. 30.3 ± 2.3 mm, $P = 0.005$, Mann-Whitney's U test).

The eye shapes were analyzed further in the remaining 114 highly myopic patients (93.2%). The frequency of the different eye shapes as expressed by the three-digit figure is shown in Figure 6. The most frequent type was 001, in which the eyes were symmetrical in the sagittal and horizontal planes, and the posterior pole was blunt (Fig. 7). This type was found in 51 of 228 eyes (23.4%). The second most frequent type was 000, in which the eye was symmetrical in the sagittal and horizontal planes, and the posterior pole was pointed (Fig. 8). This type was found in 35 of the 228 eyes (16.1%).

The type of eye shape was the same in both eyes of an individual in 61 of 117 highly myopic patients (52.1%), and was different in the remaining 56 patients. The average difference in the axial lengths between the two eyes was 1.35 ± 1.37 mm in the patients who had different shapes in the two eyes. This was significantly higher than that in patients whose eye shape was the same in both eyes (0.86 ± 0.76 mm, $P = 0.02$, Welch's t-test).

In the 56 patients whose two eyes had different shapes, the most frequent pattern of the difference was that for the pointedness of the posterior pole of the eye (the unit digit) in 29 patients (51.8%). The second most frequent pattern was for eyes that were symmetrical in the sagittal plane (the tens digit), and this was found in 25 patients (44.6%). These were followed by the difference in the degree of symmetry in the horizontal plane (the hundreds digit) in 19 patients (33.9%). The most common pair of figures in the patients who had different shapes in both eyes was the pair of "100" and "101." This pair was found in 6 of 56 patients (10.7%). The details of the pairs are shown in Supplementary Table 1 (http://www.iovs.org/lookup/suppl/doi:10.1167/iovs.12-9426/-/DCSupplemental).

All of the digits were different in 2 patients, the unit and tens digits were different in 5, the unit digit and hundreds digit were different in 6, and the tens and hundreds digits were different in 2.

Correlation between Type of Eye Shape and Axial Length and Age

We calculated the correlation between the age of the patient and the eye shape in 61 highly myopic eyes whose eye shape was the same in both eyes. There was no correlation between age and the degree of symmetry in the horizontal plane (T/N ratio), or between age and the degree of symmetry in the sagittal plane (S/I ratio). However, there was a significant negative correlation between the degree of pointedness of the eye and the patients' age ($r = -0.38$, $P = 0.003$, Spearman's correlation coefficient by rank test, Fig. 9).

There was no significant correlation between the axial length and any of the parameters (pointedness, degree of

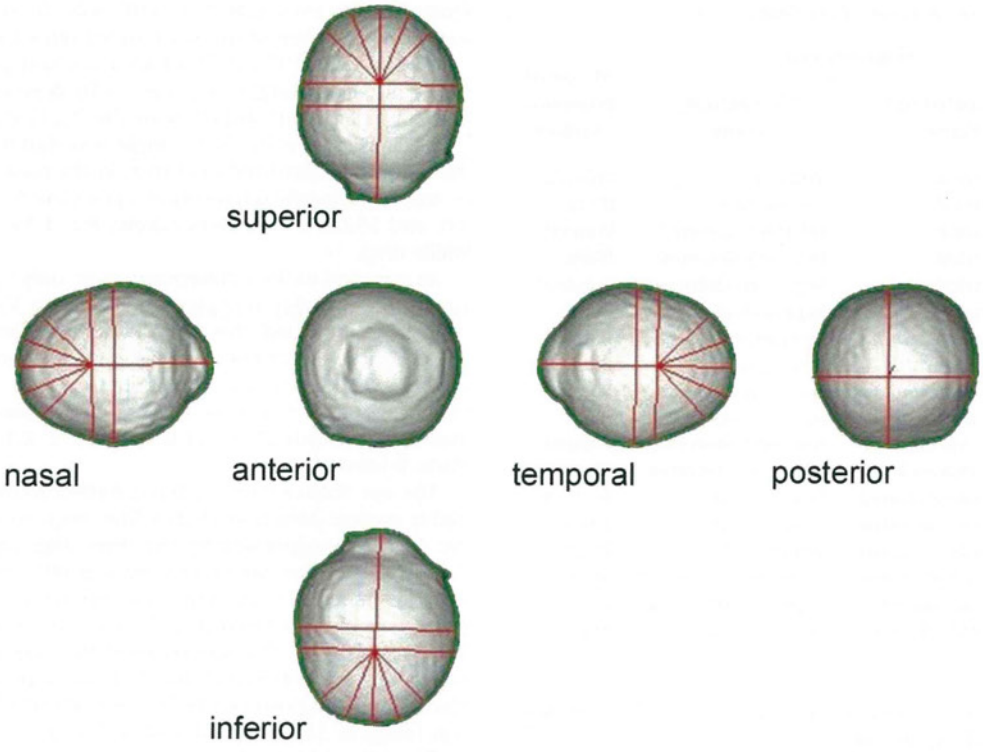

FIGURE 7. The left highly myopic eye of a 60-year-old man (axial length 33.1 mm). The V/A ratio is 81.5, the H/A ratio is 83, the T/N ratio is 96, the S/I ratio is 94, and the pointedness is 159. These data indicate that the type of ocular shape is 001.

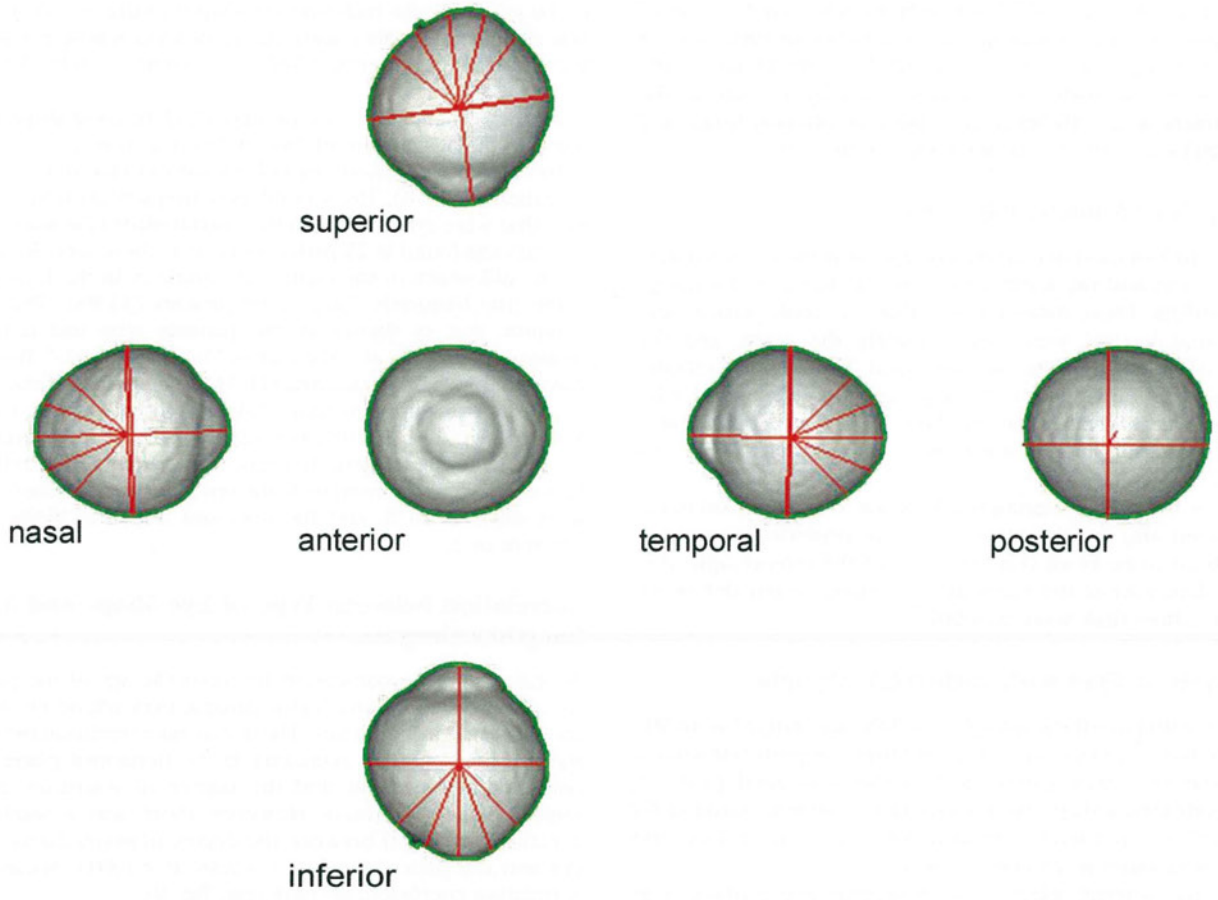

FIGURE 8. The highly myopic left eye of a 32-year-old woman (axial length 26.6 mm). The V/A ratio is 85.5, the H/A ratio is 92.5, the T/N ratio is 103, the S/I ratio is 95, and the pointedness is 147. These data indicate that the type of ocular shape is 000.

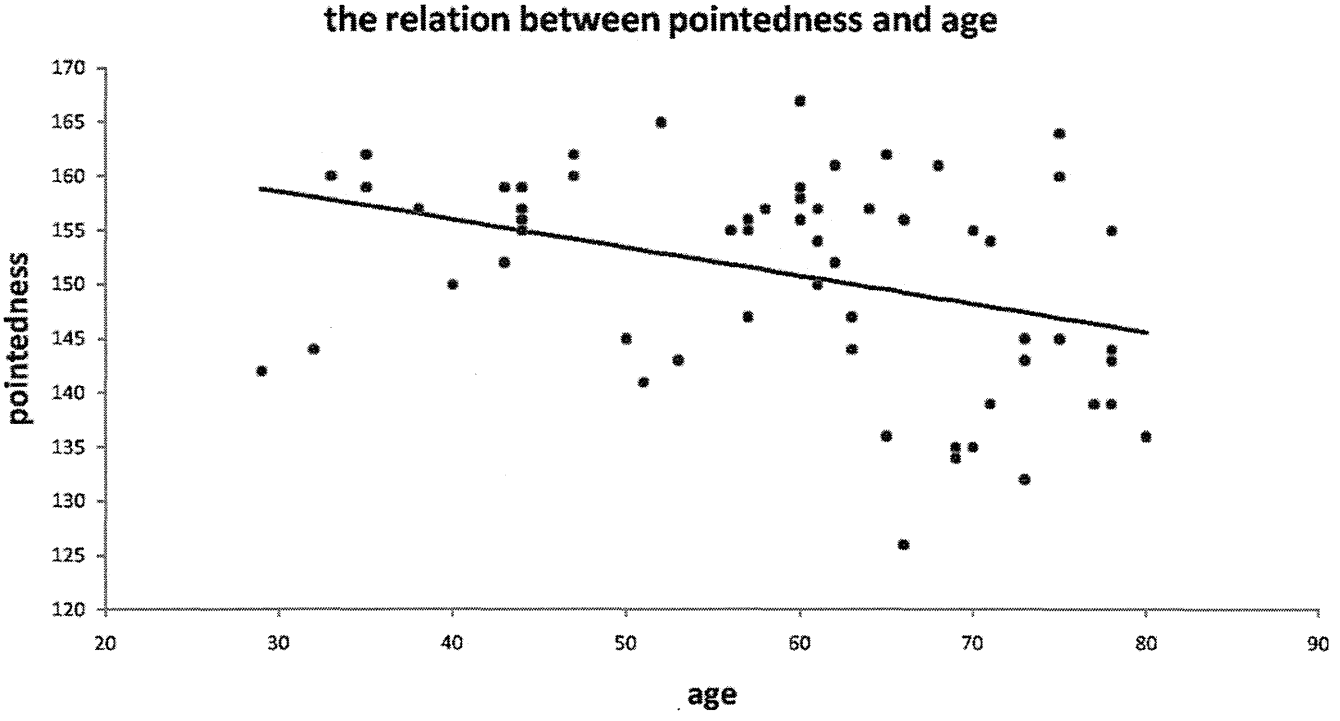

FIGURE 9. Graph showing the relationship between the degree of pointedness and the age. There was a significant negative correlation between the degree of pointedness of the eye and the patients' age ($r = -0.38$, $P = 0.003$).

symmetry in the horizontal plane, and degree of symmetry in the sagittal plane). When we divided the eyes into 2 groups according to the axial length (those with an axial length ≥30.0 mm [120 eyes] and those with an axial length <30.0 mm [114 eyes]), the number of 2's in the hundreds digit (the temporally-distorted shape) was found significantly more frequently in the eyes with a longer axial length (14.2%, 17 of 120 eyes) than in the eyes with a shorter axial length (6.1%, 7 of 114 eyes, $P = 0.04$, χ^2 test).

Association between Deformity or Symmetry and Fundus Lesions Specific to Pathologic Myopia

We examined the frequency of MTM, CNV, and chorioretinal atrophy among the different figures in each digit. The frequency of CNV was not associated significantly with the figure of each digit. On the other hand, the MTM and myopic chorioretinal atrophy were present significantly less frequently in the eyes with 0 in hundreds digit, which represents the horizontal symmetry ($P = 0.005$ and 0.04, respectively; χ^2 test), and were present significantly more frequently with a 0 in the ones digit, which is related to the pointedness of the posterior surface ($P = 4.9 \times 10^{-5}$ and 0.03, respectively; χ^2 tests).

Effects of Deformity and Symmetry on Visual Function

We then determined the absolute value of asymmetry and analyzed the effect of asymmetry on visual function. The absolute value of horizontal asymmetry was defined as the difference between T/N ratio and 100, and the absolute value of sagittal asymmetry was defined as the difference between S/I ratio and 100. Asymmetry in the horizontal and sagittal planes was not correlated significantly with the BCVA. However, the horizontal asymmetry was significantly higher in the eyes with significant visual field defects than in eyes without visual field defects ($P = 0.02$, Welch's t-tests). The visual defects were detected significantly more frequently with the number 2 in the hundreds digit, which represents temporally distorted eyes ($P = 2.2 \times 10^{-5}$, χ^2 test). The correlations between the asymmetry of the eye and patients' age or axial length were not significant.

DISCUSSION

Our results showed that our software can analyze successfully the 3D MR images of eyes quantitatively and objectively within 1 second per eye. This makes it practical to compare the eye shapes among different populations or ethnicities, and also makes it possible to follow the changes in the shape of human eyes longitudinally.

None of the emmetropic eyes met the definition of being deformed by our software analyses. In the emmetropic eyes, the axial, vertical, and horizontal lengths were not significantly different. Also, the shape of the posterior surface of the eye was symmetric horizontally and sagittally, and was classified as being blunt. Thus, we conclude that the shape of emmetropic eyes is spherical.

In contrast to the emmetropic eyes, only 2.6% of the eyes with pathologic myopia were analyzed to have no deformity by our software. The highly myopic patients whose eyes had a deformity were significantly older and had significantly longer axial lengths than those whose eyes did not have a deformity. This suggests that the deformity of the eyes with pathologic myopia increases as the patient ages, which agrees with the findings in an earlier study on highly myopic eyes observed by stereoscopic fundus examinations.[9] However, this must be confirmed in a future study with a larger number of eyes.

In the sagittal plane, 69.2% of the highly myopic eyes had a symmetric posterior surface. Of the 72 eyes whose posterior eye shape was not symmetric in the sagittal plane 66 (91.7%) had an inferiorly-deformed shape and only 8.3% had a superiorly-deformed shape. In our earlier study, we examined

the 3D MR image from the nasal side and judged the shape of the eye subjectively.[6] In that study, the part of the eye that most protruded existed along the visual axis in 78.3% of the myopic eyes, and all of the remaining eyes had the most protruded part inferior to the central axis. In our present study, the percentage of the eyes whose posterior eye shape was symmetric sagittally was slightly lower than that in our previous study,[6] and a superiorly-deformed type, which was not found in our earlier study, was identified. This difference was most likely because the current study was more quantitative and more detailed analyses of the 3D MR images were made by our software. We also had a larger number of patients.

Our results confirmed that a posterior bulge, if it existed, developed inferior to the central axis much more frequently than superior to the central axis. Very recently, Tanabe et al. reported that the choroid inferior to the optic disc was significantly thinner than that in the other sectors around the optic disc in 28 eyes with no ocular pathologies (mean refractive degree -3.6 ± 4.1 D).[10] They suggested that the thinner choroid inferior to the optic disc may be a natural anatomic architecture of normal eyes. Although it was not determined if the sclera inferior to the optic disc was thinner than other areas in normal eyes, their data in combination with our results suggest that the inferior fundus already is thinner in normal eyes and, thus, might be more susceptible to expansion in response to intraocular pressure in pathologic conditions, such as pathologic myopia or tilted disc syndrome. The precise mechanism for this phenomenon must be determined in the future.

We found that 62.4% of the highly myopic eyes were symmetric in the horizontal plane, 27.4% were nasally-distorted, and 10.3% were temporally-distorted. In our earlier study, we classified the eye shape into 4 different types (temporally-distorted, nasally-distorted, cylindrical, and barrel-shaped) based on an inferior view.[6] In that study, 36.7% had the nasally-distorted type and 16.7% had the temporally-distorted shape. Although the incidence of nasally-distorted or temporally-distorted eyes was slightly lower than that found in our current study, the difference between the two studies was not significant.

Our analyses showed that all of the emmetropic eyes had a blunt shape. Among the highly myopic eyes, on the other hand, as many as 45.7% were classified as being pointed. In addition, there was a significant negative correlation between the degree of pointedness and the patients' age (Fig. 9). This suggested that an increase in the pointedness of the posterior surface of the eye might be one important feature of eyes with pathologic myopia, and this becomes more evident as the patients age.

After classifying the eye shape into 18 types by our software, the eye shape was identical in 52.1% of highly myopic patients. This rate was lower than that of 69.8% in our previous study,[6] which probably is due to the more quantitative classification in the present study.

In patients whose eye shape was not identical between the two eyes of the same individual, the most frequent pattern of differences was the degree in the pointedness of the posterior surface of the eye. This suggests that the pointedness may be altered more easily in highly myopic eyes than the degree of horizontal or sagittal symmetry.

Finally, we calculated the absolute value of the asymmetry of the eyes and examine whether the degree of asymmetry was significantly correlated with visual function. Statistical analyses showed that the horizontal asymmetry was significantly higher in the eyes with significant visual field defects than the eyes without visual field defects. Our previous study showed that significant visual field defects were found significantly more frequently in eyes with a temporally-distorted shape.[6] Also, multiple linear regression analyses of a more recent set of data showed that the presence of an abrupt change of the scleral curvature temporal to the optic disc was the only factor associated significantly with a progression of the visual field defects.[8] These results, combined with our present data, suggest that horizontal asymmetry of the posterior surface of the eye might be a cause of optic nerve damage.

Our results also showed that the degree of pointedness was associated significantly with the degree of horizontal symmetry. The absolute value of pointedness of the posterior eye surface was significantly greater in eyes with a temporally-distorted shape than in the nasally-distorted type or horizontally-symmetrical eyes. Also, the MTM and myopic chorioretinal atrophy were present significantly less frequently in horizontally-symmetrical eyes and more frequently in eyes classified as being pointed. These findings suggested that an increased horizontal asymmetry and increased pointedness of the posterior surface shape of highly myopic eyes might be important factors that might cause the development of most of the vision-threatening complications specific to pathologic myopia, regardless of whether they develop in the papillary or macular region. A more precise mechanism of how specific types of changes in the eye shape are related to the development of myopic pathologies must be determined in a larger number of eyes with a longer follow-up period.

Our study has some limitations. This was a hospital-based study and the patients studied visited the High Myopia Clinic. Thus, it is possible that more myopic patients with vision difficulties were enrolled than existed in the general myopic population. Also, T2-weighted MRI was used, which images the intraocular fluid and not the sclera. Also, there were no follow-up data. Finally, we did not analyze the anterior portion of the eye. Thus, it is not clear whether such deformities are observed only in the posterior segment of the eye or the anterior segment of the eye also is deformed. This will be investigated in the future.

Despite these limitations, we believe that the analyses of the eye shapes with our software provided more precise and more detailed evaluations of highly myopic eyes. Further studies investigating the characteristics of human eyes, and how they are deformed in high myopes are planned. The effect of age on the eye shape, and the specific types of deformities that are correlated significantly with the vision-threatening complications of highly myopic eyes are ongoing in our institution.

Acknowledgments

Duco Hamasaki assisted with critical discussion and final manuscript revision.

References

1. He M, Zeng J, Liu Y, Xu J, Pokharel GP, Ellwein LB. Refractive error and visual impairment in urban children in southern china. *Invest Ophthalmol Vis Sci.* 2004;45:793–799.
2. Vitale S, Sperduto RD, Ferris FL 3rd. Increased prevalence of myopia in the United States between 1971–1972 and 1999–2004. *Arch Ophthalmol.* 2009;127:1632–1639.
3. Vongphanit J, Mitchell P, Wang JJ. Prevalence and progression of myopic retinopathy in an older population. *Ophthalmology.* 2002;109:704–711.
4. Logan NS, Gilmartin B, Wildsoet CF, Dunne MC. Posterior retinal contour in adult human anisomyopia. *Invest Ophthalmol Vis Sci.* 2004;45:2152–2162.
5. Atchison DA, Pritchard N, Schmid KL, Scott DH, Jones CE, Pope JM. Shape of the retinal surface in emmetropia and myopia. *Invest Ophthalmol Vis Sci.* 2005;46:2698–2707.

6. Moriyama M, Ohno-Matsui K, Hayashi K, et al. Topographic analyses of shape of eyes with pathologic myopia by high-resolution three-dimensional magnetic resonance imaging. *Ophthalmology.* 2011;118:1626–1637.
7. Kwon YH, Kim CS, Zimmerman MB, Alward WL, Hayreh SS. Rate of visual field loss and long-term visual outcome in primary open-angle glaucoma. *Am J Ophthalmol.* 2001;132:47–56.
8. Ohno-Matsui K, Shimada N, Yasuzumi K, et al. Long-term development of significant visual field defects in highly myopic eyes. *Am J Ophthalmol.* 2011;152:256–265.
9. Hsiang HW, Ohno-Matsui K, Shimada N, et al. Clinical characteristics of posterior staphyloma in eyes with pathologic myopia. *Am J Ophthalmol.* 2008;146:102–110.
10. Tanabe H, Ito Y, Terasaki H. Chorid is thinner in inferior region of optic disks of normal eye. *Retina.* 2012;32:134–139.

Association between Shape of Sclera and Myopic Retinochoroidal Lesions in Patients with Pathologic Myopia

Kyoko Ohno-Matsui,[1] Masahiro Akiba,[2] Toshio Modegi,[3] Makoto Tomita,[4] Tatsuro Ishibashi,[5] Takashi Tokoro,[1] and Muka Moriyama[1]

Purpose. The purpose of the study was to analyze the shape of the sclera determined by swept-source optical coherence tomography (OCT) and to determine the relationship between the shape and the myopic retinochoroidal lesions.

Methods. We studied 488 eyes of 272 patients with high myopia (refractive error ≥−8.00 diopters [D] or axial length >26.5 mm) and 43 emmetropic eyes of 43 controls (refractive error ≤±3 D). An image of the sclera was obtained by a swept-source OCT prototype instrument that uses a wavelength sweeping laser centered on 1 μm wavelength with an A-scan repetition rate of 100,000 Hz. The scans were 12 mm radial scans centered on the fovea. Seventy eyes were also examined by three-dimensional magnetic resonance imaging (3D MRI) to obtain the contour of the outer surface of the eyes. The main outcome measures, visibility of the entire sclera layer, scleral thickness, scleral contour, and location of the most protruded point of the globe, were obtained by swept-source OCT and 3D MRI.

Results. The entire thickness of the sclera was observed in 278 of 488 (57.0%) highly myopic eyes, but the outer border was not observed in any of the emmetropic eyes. The mean subfoveal scleral thickness was 227.9 ± 82.0 μm in the highly myopic eyes. The sclera was thickest at 3000 μm nasal to the fovea. The curvatures of the inner scleral surface of highly myopic eyes could be divided into curvatures that sloped toward the optic nerve, those that were symmetrical and centered on the fovea, those that were asymmetrical, and those that were irregular. Patients with irregular curvature were significantly older and had significantly longer axial lengths than those with other curvatures. Myopic fundus lesions were present significantly more frequently in the eyes with irregular curvature. All of the eyes whose scleral curvature sloped toward the optic nerve had nasally distorted shape in the 3D MRI images, and all eyes with temporally dislocated shape had irregular curvature.

Conclusions. In vivo evaluations of the sclera in highly myopic eyes by swept-source OCT can provide important information on deformations of the sclera and how such deformities are related to myopic fundus lesions. (*Invest Ophthalmol Vis Sci.* 2012;53:6046–6061) DOI:10.1167/iovs.12-10161

Pathologic myopia is a major cause of visual impairments worldwide.[1–6] The visual impairments are mainly caused by different types of myopic lesions in the retina and choroid, especially in the macula and optic disc areas.[7–10] However, what causes the development of these myopic lesions has not been determined, and the lack of this information has made it difficult to design therapy to reduce or prevent the development of these lesions.

To try to determine the mechanism that causes the development of myopic lesions, we analyzed the shape of the external surface of highly myopic eyes by high-resolution three-dimensional magnetic resonance imaging (3D MRI). We found that highly myopic eyes were not simply elongated but had out-pouched areas especially in the posterior pole of the eye.[11] We also found that the visual field defects[7] that were not due to a myopic fundus lesions were present significantly more frequently in eyes with temporally distorted shapes than in eyes with distortions in other areas.[11] In another study on highly myopic eyes, we found that visual field defects were observed significantly more frequently in eyes with type IX staphyloma (classification by Curtin[12]), which is the type with a ridge-like protrusion temporal to the optic disc. These findings suggested that eye shapes and deformities, especially in the posterior segment of the eye, are most likely related to the development of the myopic lesions.

We thus asked whether the shape of the sclera also was significantly associated with myopic fundus lesions. The sclera forms the principal part of the outer coat of the eye, and it helps maintain a stable ocular dimension and protects the intraocular structures. The properties of the sclera are critical in determining the size and shape of the eye.[13] The sclera consists mainly of type I collagen and is relatively avascular.[13] A histological study showed that highly myopic eyes had thinner sclera particularly at the posterior pole,[14] and the thinning was associated with a narrowing and dissociation of the collagen fiber bundles and a reduction in collagen fibril diameter.[9,14,15] Highly myopic eyes also have differences in the biochemical makeup of the sclera, such as alterations of the glycosaminoglycan and collagen content.[16] Unfortunately, these findings were made in postmortem human eyes,[17] although sclera thinning has also been observed in animal models of experimental myopia.[18–20]

From the [1]Department of Ophthalmology and Visual Science and the [4]Clinical Research Center, Tokyo Medical and Dental University, Tokyo, Japan; [2]Topcon Corporation, Tokyo, Japan; [3]Dai Nippon Printing Co., Ltd., Tokyo, Japan; and the [5]Department of Ophthalmology, Kyushu University, Fukuoka, Japan.

Supported in part by research Grants 22390322 and 23659808 from the Japan Society for the Promotion of Science, Tokyo, Japan.

Submitted for publication May 7, 2012; revised June 19 and July 17, 2012; accepted July 28, 2012.

Disclosure: **K. Ohno-Matsui**, None; **M. Akiba**, Topcon Corporation (E); **T. Modegi**, None; **M. Tomita**, None; **T. Ishibashi**, None; **T. Tokoro**, None; **M. Moriyama**, None

Corresponding author: Kyoko Ohno-Matsui, Department of Ophthalmology and Visual Science, Tokyo Medical and Dental University; 1-5-45 Yushima, Bunkyo-ku, Tokyo 113-8510, Japan; k.ohno.oph@tmd.ac.jp.

Investigative Ophthalmology & Visual Science, September 2012, Vol. 53, No. 10

In spite of the importance of the sclera in determining the size and shape of the eye, detailed information on the biometrics of the sclera is limited, and the information published has been mainly obtained from postmortem tissues. Thus, it is difficult to extend these findings to the eye in situ and to determine the relationship of these findings to the development of myopic lesions.

Recent advances in optical coherence tomography (OCT) have enabled investigators to image the tissues deeper than the neural retina such as choroid and sclera. A PubMed search identified only two articles reporting on the appearance of the sclera in the macular area obtained by OCT.[21,22] In one paper, Imamura et al.[21] reported the use of enhanced-depth imaging OCT (EDI-OCT), and showed that the subfoveal sclera was significantly thicker in highly myopic eyes with a dome-shaped macula (DSM), a protrusion of the macula within a staphyloma,[23] than in highly myopic eyes without a DSM. Maruko et al.[22] measured scleral thickness in the posterior fundus in the images obtained by a prototype swept-source OCT in nine patients with the tilted-disc syndrome (TDS) with a mean axial length of 24.89 ± 1.05 mm. They reported that the subfoveal sclera was significantly thicker than the sclera superior and inferior to the fovea. Both of these studies showed that in vivo observations of the sclera of human eyes can be made by OCT.

Swept-source OCT is a relatively new instrument that uses a wavelength-sweeping laser as the light source[24] and has less sensitivity roll-off with tissue depth than conventional spectral-domain OCTs. The current swept-source OCT instruments use a longer central wavelength, generally in the 1 μm range, which has improved their ability to penetrate deeper into tissues than the conventional spectral-domain OCT instruments. With this deeper penetration, evaluations of the choroid and sclera are potentially possible.

Because we are interested in determining the mechanism causing myopic fundus lesions, we have been examining the morphology of the deeper tissues in the macular and peripapillary regions of highly myopic eyes in patients in our High Myopia Clinic by swept-source OCT.[25–28] We argue that swept-source OCT will provide more detailed images of the choroid and sclera even though the scanned area is smaller and more limited than with MRI. Swept-source OCT has the advantage of enabling the user to analyze the spatial relationship between the morphology of the retina/choroid and the myopic fundus lesions because it can show different eye structures in the same scan. We expected that this information would provide clues to how such deformities can lead to vision-threatening lesions specific to pathologic myopia.

Thus, the purpose of this study was to analyze the morphological features of the sclera in the posterior pole and to analyze the scleral contour in a large number of highly myopic eyes by swept-source OCT. We showed that the entire layer of the sclera was clearly visible in 57% of the highly myopic eyes and that the contour of the sclera can be divided into four distinct patterns. Examinations of the four patterns showed that some were significantly associated with myopic lesions. We also compared the shape of the eye obtained by swept-source OCT to that obtained by 3D MRI. These results showed not only that the shape of highly myopic eyes is distorted but also that the distortions are related to the development of vision-threatening complications in patients with pathologic myopia.

Methods

The procedures used in this research adhered to the tenets of the Declaration of Helsinki and were approved by the Ethics Committee of Tokyo Medical and Dental University. A written informed consent was obtained from all participants for the original examination procedures.

Two hundred seventy-two consecutive patients with pathologic myopia were evaluated by swept-source OCT from May 6, 2011, to December 9, 2011, in the High Myopia Clinic at Tokyo Medical and Dental University, Tokyo. The definition of pathologic myopia was a refractive error (spherical equivalent) >−8.00 diopters (D) or an axial length >26.5 mm. Forty-three eyes of 43 subjects with refractive errors ≤±3 D were classified as emmetropic and were examined in the same way. All of the emmetropic participants were current or former staff members of our university and all volunteered. Patients whose swept-source OCT images were of poor quality due to a dense cataract, poor fixation because of macular chorioretinal atrophy, or myopic macular holes were excluded. Patients with a history of vitreoretinal surgery were also excluded because such surgery could affect the scleral contour.

All of the participants had a comprehensive ocular examination including measurements of the refractive error (spherical equivalent), axial length with the IOLMaster (Carl Zeiss Meditec, Dublin, CA), and fundus biomicroscopy. The presence of a posterior staphyloma was determined by stereoscopic fundus examinations.

Swept-Source OCT

All the eyes were examined by a prototype swept-source OCT instrument manufactured by Topcon Corporation (Tokyo, Japan). This OCT system has an A-scan repetition rate of 100,000 Hz, and its light source is a wavelength-sweeping laser centered at 1050 nm with an approximate 100 nm bandwidth, although the effective bandwidth was approximately 60 nm because of water absorption. The axial resolution was calculated to be 8 μm in tissue with a lateral resolution of 20 μm. The imaging depth was 2.6 mm in tissue, and the lateral scan length was adjustable. For our scanning protocol, 12 mm scans along 12 meridians centered on the fovea were performed. A single image was made up of 1024 A-line scans acquired in 10 ms. Typically, 32 B-scan images were recorded and averaged by postprocessing to yield a despeckled high-quality B-scan image.

The central retinal thickness was measured with the caliper function of the built-in software of the OCT. The scleral thickness was measured at the fovea and at four different areas: 3 mm superiorly, inferiorly, temporally, and nasally to the fovea. These measurements were made by one masked author (MM). Because the choroid was too thin to be measured in many highly myopic eyes, the number of eyes whose choroid was too thin to be measured was counted instead.

The contour of inner scleral surface, the chorioretinal interface, was outlined manually in each eye, and the eyes were classified according to their contour. In some eyes with pathologic myopia, the peak of the curvature of the posterior segment did not correspond to the center of the fovea. In these eyes, the most posteriorly protruded point in the fundus was identified. The most protruded part was identified in each of 12 radial scans centered on the central fovea, and the depth of the most protruded part from the foveal plane was measured in each scan (Fig. 1A). Then the scan that included the most protruded part was determined. The distance of the most protruded point from the fovea as well as the depth of the most protruded point from the foveal plane was measured with the caliper function of the built-in software of the OCT by one masked author (MM). For the distribution of the most protruded point, we combined the superior, superior–temporal, and superior–nasal findings and called this segment the upper quadrant, and we also combined the lower, temporal–lower, and nasal–lower findings and called this segment the lower quadrant (Fig. 1B).

Analysis of Eye Shape by High-Resolution 3D MRI

We recently reported that it was possible to obtain a complete topographic image of human eyes by high-resolution 3D MRI.[11] We compared the contour of the inner scleral surface seen in the OCT

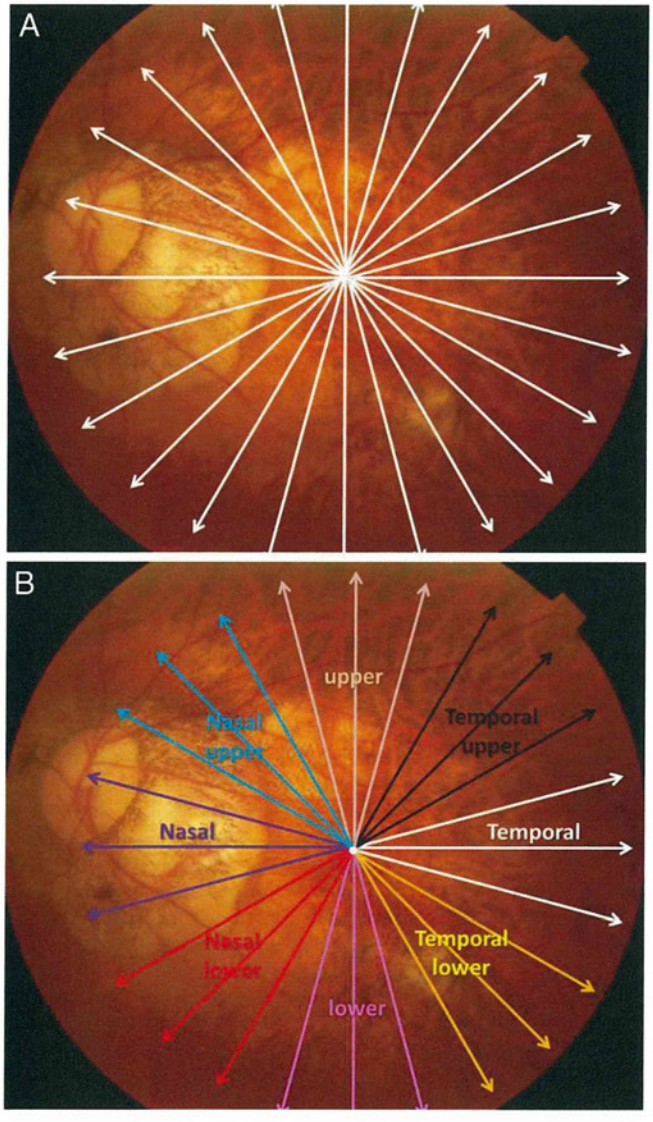

FIGURE 1. Area scanned by swept-source OCT superimposed on fundus photograph. (**A**) Area scanned by 12 mm meridian scans centered on the central fovea. The angle between each pair of scans is 15°. (**B**) Classification of the 12 meridian scans into eight categories according to their orientations.

images and the shape of the outer surface of the eye obtained by 3D MRI. We have developed software to analyze the human eye shape obtained by 3D MRI, and we used this software to automatically analyze the degree of symmetry of the posterior eye segment in the horizontal and sagittal planes. We also determined the pointedness or bluntness of the posterior pole of the eye (Fig. 2). Briefly, the view of the eyes from six points, namely the front, back, superior, inferior, nasal, and temporal, was incorporated into the software of the 3D MRI. Then, a central axis line passing through the geometric center of the eye was automatically drawn. The point of intersection of the central axis and the posterior margin of the eye was defined as the basal point (P_b). Then, a point on the central axis 87 pixels, approximately 12.5 mm, anterior to the P_b was defined as the point of origin (P_o) of the measurements; the purpose was to avoid the influence of axial length on the location of P_o.

Next, P_o was rotated 22.5° nasally in the horizontal plane, and a line was drawn posteriorly. Where the line intersected the margin of the eye was called P_n. Similarly, P_o was rotated 22.5° temporally in the horizontal plane, and where the line from P_o intersected the margin of

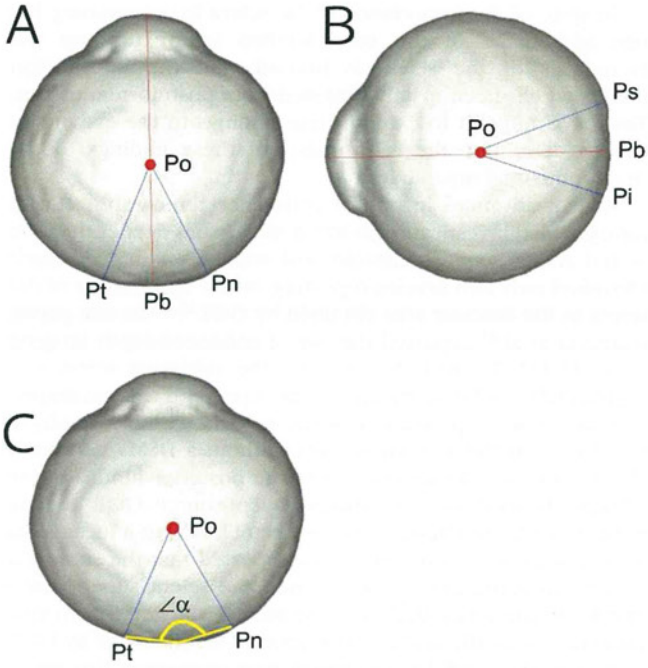

FIGURE 2. Degree of symmetry and pointedness of the posterior segment of the eye obtained by 3D MRI. (**A**) Inferior view from which the horizontal symmetry was determined. The point of intersection between the central axis and the posterior edge of the eye was defined as the basal point (P_b). Then, the point on the central axis 87 pixels away from P_b was defined as the measurement point of origin (P_o). Next, the point that was rotated 22.5° nasally (P_n) or temporally (P_t) was determined. The area of the arc surrounded by P_o, P_b, and P_n was defined as S_n; the area of the arc surrounded by P_o, P_b, and P_t was defined as S_t; the area of the arc surrounded by P_o, P_b, and P_i was defined as S_i; and the area of the arc surrounded by P_o, P_b, and P_s was defined as S_s. The horizontal symmetry is given by the ratio of S_n and S_t. (**B**) The sagittal symmetry was determined by the nasal view of the 3D MRI image. P_b and P_o were determined as described for (**A**). The point that was rotated 22.5° superiorly (P_s) or inferiorly (P_i) was determined. The area of the arc surrounded by P_o, P_b, and P_i was defined as S_i, and the area of the arc surrounded by P_o, P_b, and P_s was defined as S_s. The sagittal symmetry is given by the ratio of S_i and S_s. (**C**) The angle $<P_n$-P_b-P_t was defined as the posterior sharpness.

the eye was called P_t. In the sagittal plane, P_o was rotated either inferiorly or superiorly, and where lines intersected margin of the eye was called P_i or P_s, respectively. The area of the segment formed by P_o, P_b, and P_n was defined as S_n; the area of the segment formed by P_o, P_b, and P_t was defined as S_t; the area formed by P_o, P_b, and P_i was defined as S_i; and the area formed by P_o, P_b, and P_s was defined as S_s. The degree of symmetry in the horizontal plane was expressed by the ratio of S_n and S_t, and the degree of symmetry in the sagittal plane was expressed by the ratio of S_i and S_s. The posterior surfaces with ratios between 90 and 110 were classified as symmetrical.

For the sharpness of the posterior surface, the angle formed by P_n, P_b, and P_t was defined as the posterior sharpness angle. The shape of the posterior segments of the globe was defined as "pointed" when this angle was $\leq$150°, and the shape of posterior segment of the eye was defined as "dull" when this angle was >150°.

Statistical Analyses

The patients' age, refractive error, axial length, central retinal thickness, and scleral thickness were compared between eyes whose entire scleral layer was visible and those whose entire scleral layer was not visible in the OCT images by Welch's *t*-tests and Student's *t*-tests. The number of eyes whose choroid was too thin to be measured and the prevalence of a posterior staphyloma were compared between

Table 1. Demographics of Patients with Pathologic Myopia

Sex, No. of eyes (No. of persons)	
Men	131 (75)
Women	357 (197)
Age, y, mean ± SD	57.1 ± 13.8 (12–89)
Refractive error, d, mean ± SD	−13.3 ± 4.1 (−8.5 to −25.5)
Axial length, mm, mean ± SD	29.9 ± 2.0 (26.6–36.6)
Posterior staphyloma, No. of eyes (%)	
Present	412 (84.4%)
Absent	76 (15.6%)

groups using Fisher's exact probability tests or χ^2 tests. The clinical characteristics of eyes with the four distinct patterns of curvature of the posterior fundus were analyzed using one-factor analysis of variance (ANOVA). The correlation between the subfoveal scleral thickness and the patient's age and axial length was analyzed using Pearson tests for rank correlation coefficients. For bilaterally affected eyes, one eye was randomly selected using random number tables for statistical analyses. A P value < 0.05 was considered statistically significant.

Results

Five hundred forty-four eyes of 272 consecutive patients were examined in our High Myopia Clinic, and these patients also underwent swept-source OCT. Of these 544 eyes, 56 eyes were excluded because of poor fixation during the OCT examination due to large macular atrophy (35 eyes), low-quality OCT images due to dense cataracts (5 eyes), or history of vitreoretinal surgery (6 eyes). The remaining 10 eyes were excluded because these eyes were not highly myopic in these patients with unilateral high myopia. In the end, 488 eyes of 272 highly myopic patients were studied; their demographics are shown in Table 1. A posterior staphyloma was present in 412 eyes (84.4%) and was absent in 76 eyes (15.6%).

Swept-Source OCT Findings for Sclera in Eyes with Pathologic Myopia

The sclera was observed as a relatively uniform hyperreflective structure exterior to the thin choroid in the swept-source OCT images (Fig. 3). We were also able to observe the retrobulbar orbital fat beyond the sclera in eyes with pathological myopia. A close observation of the deeper tissues showed a relatively hyporeflective layer outlining the sclera (Fig. 3). This hyporeflective layer was in close contact with the outer surface of the sclera and appeared to break up into smaller bundles and blend into the orbital fat tissue posteriorly (Figs. 3E, 3F). The hyporeflective layer was considered to be the episclera and Tenon's capsule.[13] In some scans, cross sections of episcleral blood vessels were observed posterior to the sclera (Fig. 3E).

Factors Significantly Correlated with Visibility of Entire Sclera

To be able to measure the sclera thickness, it was necessary to determine whether the entire sclera was visible in the swept-source OCT images. Our findings showed that the entire scleral layer was observed in all 12 radial scans in 278 of 488 eyes (57.0%) and not observed in any of the 12 radial scans in 180 of 488 eyes (36.9%). A DSM, a convex elevation of the macula that differed from a surrounding staphyloma,[21,23] was observed in 93 of 488 eyes. In 32 of these 93 eyes, the entire scleral layer was visible in all 12 radial scans; in the other 31 eyes, the outer border of the sclera was visible in none of the scans. In the remaining 30 eyes, the sclera in the macular area was too thick to allow a view of the outer border of the sclera due to the DSM, although the entire scleral layer was visible in areas outside the DSM area.

The clinical characteristics of the 278 eyes of 175 patients whose entire scleral layer was visible in all 12 radial scans, as well as those of the 180 eyes of 114 patients whose outer scleral border was not visible in any of the 12 radial scans, are shown in Table 2. In 17 patients, the entire scleral layer was visible in one eye but not visible in the fellow eye. The patients whose entire scleral layer was visible were significantly older, were significantly more myopic, and had significantly longer axial lengths than those whose entire scleral layer was not visible (Table 2).

A posterior staphyloma was present in all 278 eyes whose entire scleral layer was visible, whereas a staphyloma was found in 57.8% of the 180 eyes whose entire scleral layer was not visible ($P < 0.05$, Fisher's exact probability tests).

Sixty-five of 278 eyes whose entire scleral layer was visible were excluded from the central retinal thickness measurements: 44 eyes due to macular retinoschisis, 2 eyes due to macular holes, 4 eyes due to macular atrophy, and 15 eyes due to myopic choroidal neovascularization (CNV). Similarly, 15 of 180 eyes whose entire scleral layer was not visible were excluded from the measurements of central retinal thickness: 8 eyes due to macular retinoschisis, 1 eye due to macular atrophy, and 6 eyes due to myopic CNV. In the end, the central retinal thickness was compared between 213 of 278 eyes whose entire scleral layer was visible and 165 of 180 eyes whose entire scleral layer was not visible.

The results showed that the central retina in the eyes whose entire scleral layer was visible was significantly thinner than in those whose entire scleral layer was not visible (Table 2). There was a significant negative correlation between central retinal thickness and axial length ($r = -0.19$, $P = 0.0007$, Pearson's correlation coefficient test), while the correlation was not significant between central retinal thickness and the age of the patient.

In many eyes with pathologic myopia, the subfoveal choroidal thickness was too thin to measure. Thus, we counted the number of eyes whose subfoveal choroid was too thin and compared the frequencies between the eyes where the entire sclera layer was visible and those in which the entire sclera layer was not visible. This measurement was made by one masked author (MM). The subfoveal choroid was too thin to be measured in 239 of 278 eyes (86.0%) whose entire layer of sclera was visible; this was the case significantly more frequently than in the eyes whose entire scleral layer was not visible (29 of 151 eyes [16.1%]) ($P = 1.5 \times 10^{-48}$, χ^2 tests).

Scleral Thickness in Different Regions of Posterior Pole in Highly Myopic Eyes

We measured the scleral thickness in different regions of highly myopic eyes whose entire scleral layer was visible in all 12 meridians in the OCT images. We excluded 32 of 278 eyes with a DSM. Thus, 246 eyes were analyzed, and the mean subfoveal scleral thickness was 227.9 ± 82.0 μm, with a range of 80 to 546 μm in these eyes. The subfoveal scleral thickness was significantly correlated with the axial length ($r = -0.35$, $P = 2.8 \times 10^{-7}$, Pearson tests for rank correlation coefficients), but the subfoveal scleral thickness was not significantly correlated with the age of the patient.

Scleral thickness was also measured in the 246 eyes at 3 mm temporal, superior, and inferior to the fovea. The scleral thickness was not measured at 3 mm nasal to the central fovea in 29 eyes because of the presence of a scleral ridge temporal

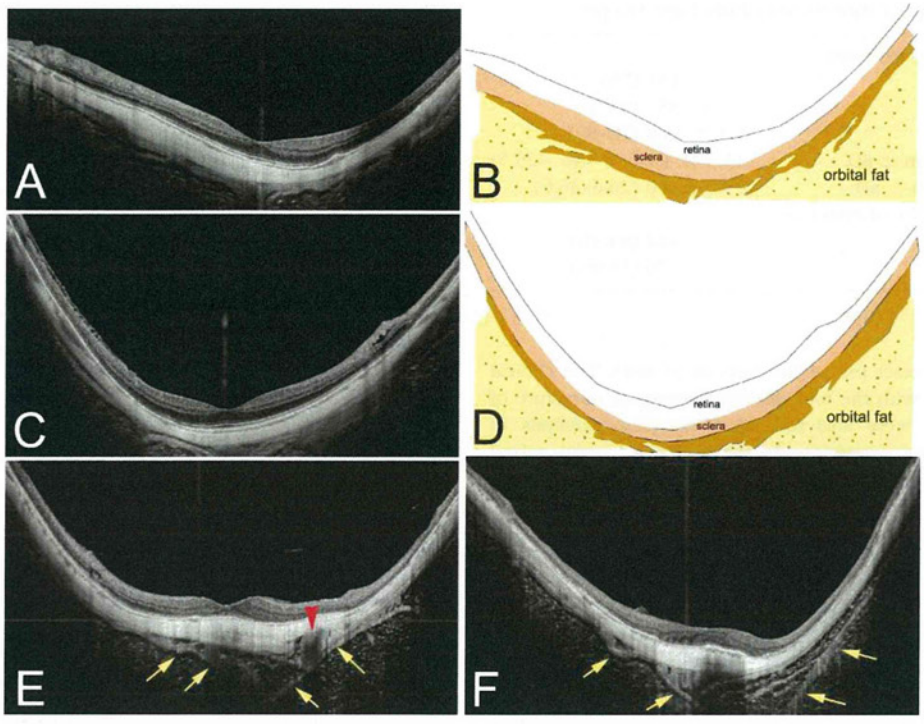

Figure 3. Observations of the sclera and Tenon's capsule in highly myopic eyes by swept-source OCT. (**A**, **C**) The sclera is observed as the highly reflective tissue outside the very thin choroid. A less reflective tissue can be seen outside the sclera. Orbital fat tissue is also observed as grayish tissue with many dots. (**B**, **D**) Schematic drawings of (**A**) and (**C**), respectively, with the tissues labeled. The sclera is colored *orange* and the tissue outside the sclera, suggestive of Tenon's capsule and episclera, is colored *brown*. (**E**, **F**) The fibers (*arrows*) of Tenon's capsule appear to spread and blend into the orbital fat tissue posteriorly. Cross sections of episcleral blood vessels can be seen posterior to the sclera (*arrowhead*, **E**).

to the optic disc due to type IX staphyloma.[12,29] The mean scleral thickness was 190.7 ± 71.6 μm with a range of 65 to 488 μm at 3 mm superior to the central fovea, 182.7 ± 70.2 μm with a range of 53 to 414 μm inferior, 181.8 ± 75.1 μm with a range of 45 to 453 μm temporal, and 252.8 ± 90.8 μm with a range of 74 to 513 μm nasal to the fovea. Statistical analyses showed that subfoveal scleral thickness was significantly greater than that at 3 mm temporal to the fovea, than that at 3 mm upper to the fovea, and than that at 3 mm lower to the fovea ($P < 0.001$, paired *t*-tests). The subfoveal scleral thickness was significantly less than that at 3 mm nasal to the fovea ($P < 0.001$, paired *t*-tests). In fact, the sclera at 3 mm nasal to the central fovea was significantly thicker than that at the subfoveal, temporal, superior, and inferior regions ($P < 0.001$, paired *t*-tests). The scleral thickness was not significantly different between the temporal area and the area superior to the fovea, between the temporal area and the area inferior to the fovea, or between the areas superior and inferior to the fovea.

When all these findings are combined, the sclera was thickest in the area nasal to the central fovea, followed by the subfoveal area, and then by the areas temporal, superior, and inferior to the fovea.

Four Different Types of Curvature of Inner Scleral Surface of Highly Myopic Eyes

In emmetropic eyes, the curvature of Bruch's membrane was not similar to the curvature of the inner scleral surface mainly because the choroid was thick and the choroidal thickness

Table 2. Comparison of Clinical Characteristics between Highly Myopic Eyes Whose Entire Scleral Layer was Visible and Those Whose Entire Scleral Layer was not Visible

	Visibility of the Outer Border of Sclera		
	Yes, in All 12 Radial Scans	**No, in None of the 12 Radial Scans**	***P* Value**
No. of eyes (No. of persons)	278 (175)	180 (114)	
Age, y, mean ± SD	60.9 ± 11.4 (32-89)	54.1 ± 16.4 (12-85)	0.0006*
Refractive error, d, mean ± SD	−15.1 ± 4.3 (−8.5 to −25.5)	−11.4 ± 3.0 (−8.5 to −18.5)	<0.0001†
Axial length, mm, mean ± SD	30.7 ± 1.9 (26.5-36.6)	28.2 ± 1.9 (26.5-32.5)	<0.0001†
Posterior staphyloma, No. of eyes (%)			
Present	278 (100%)	104 (57.8%)	<0.05‡
Absent	0 (0%)	76 (42.2%)	
Central retinal thickness, μm, mean ± SD	140.5 ± 35.4 (59-230)	158.5 ± 36.8 (52-253)	<0.0001†

* Welch's *t*-tests.
† Student's *t*-tests.
‡ Fisher's exact probability tests.